RESEARCH

Does time series analysis confirms the relationship between space weather effects and the failures of electrical grids in South Poland?

Agnieszka Gil[1][*] , Renata Modzelewska[1], Szczepan Moskwa[2], Agnieszka Siluszyk[1], Marek Siluszyk[1], Anna Wawrzynczak[3] and Sylwia Zakrzewska[4]

[*]Correspondence: gila@uph.edu.pl
[1]Institute of Mathematics and Physics, Siedlce University, Siedlce, Poland
Full list of author information is available at the end of the article

Abstract

Nowadays, when the global and national industry is addicted from various electrical and electronic equipment at a very high level, it is of a special interest to understand the possible origins of the interruptions in the electricity supply. Failures in ground-based electrical and electronic systems, or disturbances of satellites operation caused by influential magnetic storms initiated by the changeable Sun can have a high economic impact on the industry. These strong magnetic storms are triggered by solar-driven disturbances in interplanetary space. Studies of these phenomena have gained a special attention since the incident that had occurred in northern Canada in March 1989. During this event the work of the hydroelectric plant in the region of Quebec was blocked for long, winter hours and many citizens of this region of Canada suffered from a blackout. Analysis performed in the Oak Ridge National Laboratory showed that if that blackout have had taken place in the USA then costs generated only by a not supplied electricity could even reach 6 billion USD.

In our paper, we apply time series and statistical analysis tools, i.e. superposed epoch analysis and Wilcoxon Matched Pairs Test, for a large set of data, among them: 4625 failures of electrical grids in southern Poland in 2010, from the total number of 25,616, and 10,656 in the first seven months of 2014, from the total number of 30,155. We investigate only those failures which might be connected with the above described effects. We analyze data of breakdowns with unidentified reasons, as well as failures connected to the aging and electronic devices breakdowns, which occurred during the periods of an increased geomagnetic activity. Based on the data from The Institute of Meteorology and Water Management-National Research Institute we eliminate from the consideration those failures which had meteorological grounds. Our analysis shows the usefulness of these mathematical tools in such a vital for the global and national industry issue, as well, that powerful phenomena of solar origin, somewhat disturbed in 2010 and January–July 2014 the electrical grids productivity in southern Poland.

Keywords: Time series analysis; Space weather; Geomagnetically induced currents; Electrical grids

1 Introduction

Our Sun is not a constant body. Its behavior changes in various scales. Solar activity (SA) is usually characterized by a number of sunspots emerging on the solar surface, varying in time. The 11-year solar cycle (from one minimum to the next minimum epoch of SA) shows temporal changes of the level of SA. The 22-year solar magnetic cycle is associated with the reversal of the Sun's global magnetic field in the maximum epoch of SA. At the maximum epochs (a period with a peak in the sunspot number), the polarity of the Sun's global magnetic field reverses, so that the North magnetic pole becomes the South and vice versa. Accordingly, there exists the 22-year solar magnetic cycle. As a consequence, the 22-year solar magnetic cycle consists of two different polarity periods (from one maximum to another maximum epoch of SA), each lasting 11 years. When the global magnetic field lines are directed outward from the northern hemisphere of the Sun and are directed backward to southern hemisphere, this 11 year part of the 22-year solar magnetic cycle called the positive ($A > 0$) magnetic polarity epoch, while in vice versa case, it is called the negative ($A < 0$) magnetic polarity epoch [1].

The exceptional phenomenon of the activity of Sun is solar wind- an extension of the outer atmosphere of the Sun (solar corona) into interplanetary space [2], changing in time and having the asymmetrical distribution with the heliolongitudes, especially during the solar minimum. The space around the Sun, where the solar wind dominates, is called the heliosphere.

Sun is also a source of the outstanding solar flares (SFs) and the coronal mass ejections (CMEs) causing the powerful disturbances in the interplanetary space. They appear in time by chance, sporadically, without any regularity, increasing its frequency in the maximum epochs of SA. Consequently, the interplanetary space is fulfilled with the electromagnetic fields consisting of the regular and turbulent components developing dynamically with different time and spatial ranges. Thus, Earth's environment is affected by the solar-driven effects, commonly known as space weather. The term space weather refers to conditions on the Sun and in its atmosphere, as well as, in the heliosphere that can influence the space born and ground based technological systems [3] and human existence [4].

Variability of the Sun [5], continuously measured from 17th century, influences the Earth in a number of ways, depending on the level of solar activity. Various phenomena occurring on the Sun lead to a transformation of solar magnetic energy into space-weather-driving incidents. During the solar maximum transient phenomena, as above-mentioned solar flares and coronal mass ejections are very frequent, and lead to an increase in the injection, acceleration, and transportation of solar energetic particles (SEPs).

Interactions of Sun-induced-phenomena with the Earth's magnetic field can lead to a geomagnetic storm. Strong magnetic storm affects the normal operation of ground located electrical systems and causes damages of satellites and its equipment, which impacts satellite phones, GPS systems etc. Geomagnetic storms are classified by the planetary geomagnetic Kp index values. According to the National Oceanic and Atmospheric Administration Space Weather Geomagnetic Storms Scale (http://www.swpc.noaa.gov) when $Kp = 5$, then it is G1 minor geomagnetic storm, for $Kp = 6$, then it is G2 moderate storm, $Kp = 7$: G3 strong, $Kp = 8$: G4 severe, and $Kp = 9$: G5 extreme geomagnetic storm. [6] formulated the following geomagnetic storm criteria: long duration (>3 hours), large and negative B_z HMF component (< -10 nT) events, linked with interplanetary duskward electric fields > 5 mV/m. They found a one-to-one relationship between these interplane-

tary events and intense geomagnetic storms, and recommended that these conditions can be used in the geomagnetic storm predictions.

Among the main space weather effects [3] are: radio blackouts, solar radiation storms, and geomagnetic storms. Usually the real space weather event is the mixture of the above mentioned phenomena, with complex temporal and spatial distribution. Radio blackout is caused by SF, when X-ray emission increases low altitude ionization. As a consequence it is observed the absorption and disruption of high frequency (HF) radio waves (3–30 MHz). HF radio blackouts are especially frequent in polar regions. It can affect the proper operation of aviation and shipping, as well as the military systems [7].

Over the past decades many investigators studied the possible effects of extreme space weather phenomena on electricity transmission infrastructure, e.g. [7–9], but non of them concerned Polish energy infrastructure. Particularly, space weather effects may disturb infrastructure, such as transformers, required to operate electricity transmission and announce voltage instabilities that consequently protect the power system assets from damage. Also satellites are unsafe [10], because energetic electrons trapped in the outer radiation belt, causing electrostatic charging and discharging, can damage electronics and solar panels. Fortunately, total destruction is quite rare, because satellites are planned to accept a total dose over some lifetime, with good safety limitations: temporary outages and fleet aging are both more probable [7].

During solar radiation storms SEPs are accelerated by SFs and CMEs. Flux of energetic particles can influence not only technological systems (e.g. the electronic devices on satellites, aircraft, etc.) [11], but also has an impact on the human existence (astronauts, aircrew, and airline passengers) [3].

Geomagnetically induced currents (GIC) are a phenomenon initiated by the interaction between space weather and the Earth's magnetic field. As a powerful geomagnetic storm penetrates the Earth's magnetosphere, it can result in a high current electrojet in the ionosphere. The electrojet can reach several million amperes. This current varying with time induces a geoelectric field. The geoelectric field causes a current to flow in the same direction, being recognized as GIC, e.g. [12]. In regions of increased ground resistivity the current will flow through power lines [8, 9], gas pipelines [13, 14] or other available conductive media, such as railways. For gas pipelines, GIC can cause a variation in the pipe to soil voltage which can disturb the cathodic protection system [9]. During the extreme geomagnetic storms, GIC can disrupt transmission systems. Extreme GICs can directly damage transformers through spot heating [3]. The transformer damage can have substantial financial consequences because it can potentially leave areas without power for a long time, as well as incurring the cost of replacing the transformer. In [9] it was shown that high geomagnetic latitudes (greater than 60°), where geomagnetic disturbances are more significant and more frequent, are at particular risk from GIC. Although, it has to be underlined that at low and mid-latitude countries GIC can cause the failure of transformers through repeated heating of the transformer insulation [15, 16].

The development of current knowledge about the influence of GIC on power systems was caused mainly based on the analyses of historical events. The most recognized event happened in Canada in the March 1989 storm [17]. At 2:44 *a.m.* on *March* 13, 1989 a 100 ton static VAR capacitor at Chibougamau sub-station, Quebec, Canada, tripped and went off-line due to GIC causing a protective relay to sense overload conditions. The tripped VAR capacitor caused a cascade of failures throughout the Quebec power

grids; most notably five transmission lines from James Bay were tripped causing a loss of 9450 MW. The total load in the grid at the time was about 21,350 MW. A mere 75 seconds after the first capacitor went down most of the province was left without power. Automatic load reduction systems tried to restore balance in the power system by disconnecting towns and regions but failed. This cascade of spreading failures was much too fast for any meaningful form of manual intervention by operators to take place. 6 million of Hydro-Quebec customers were left without power for up to 9 hours. The total cost of repairs and replacement electricity for the owner Public Service Electric and Gas was later estimated to be above US$20 million [18, 19].

The second well-known event is the Halloween Storm, on *October* 30, 2003. Two CMEs hit Earth close to each other in time resulting in *Kp* = 9 events with peak geomagnetic *Dst* index values of −383 nT. The first CME erupted from the Sun at 11:10 (UTC) on the 28th of *October* 2003 and hit Earth about 19 hours later at roughly 06:10 (UTC). The second CME erupted at 20:49 (UTC) and reached Earth at 16:20 (UTC). At 20:04 (UTC) the storm peaked and the geoelectric field reached values of 2 V/km in the Malmo region [12]. This storm had a wide array of consequences for different technological systems. In Sweden on *October* 30 21:07 (local time, UTC + 1), a blackout occurred that lasted for 20–50 minutes and affected 50 000 customers in Malmo and surrounding areas. The root cause was a relay in the 130 kV system [12]. The same storm is reported to have caused significant transformer damage in South Africa. Over 15 transformers in South Africa were damaged during this period, some beyond repair [4, 15]. Among other affected systems can be mentioned, the Wide Area Augmentation System (WAAS), a navigation system based on GPS, operated by the Federal Aviation Administration, which was out of service for 30 hours and also the ADEOS-2 satellite that was severely damaged due to the storm [18].

Particularly, it is worth mentioning that on 29th *October* 2003, at 07:46 an import from Poland to Sweden via SwePol Link of 300 MW energy was disrupted. Similarly, on 20th of *November* 2013, at 18:04 SwePol Link 400 kV line tripped disrupting an import from Poland of 400 MW [19, 20].

The described above cases of energy infrastructure failures make society aware that geomagnetic storms, and hence GIC, are the results of a very complicated sequence of events, originating from magnetic energy accumulated in the Sun's interior. This energy is transferred via interplanetary space, the magnetosphere, the ionosphere, the ground to finally end up as a quasi-DC current flowing through transformers in the power systems. Since transformers are generally not designed to handle DC current flowing through the neutral point, this causes problems. The resultant saturation of the transformer core is the source of all primary risks to the power system [19]. Developing and maintaining the national power systems it must be taken into account that geomagnetic storms are very real social treats and have a potential to cause substantial damage both, to the power system and to other critical infrastructures. If not properly handled the socioeconomic consequences can be severe. Thus, it is crucial to analyze applying various mathematical and statistical tools, does and in what extent, the Polish energy infrastructure is affected by the space weather outcomes. Such an analysis is presented in the next sections of this paper. It is worth mentioning that time series analysis tools are often used in the studies of space weather issues [21–25], but for the first time are used to portray connections between the Polish energy infrastructure elements' failures and geoeffective incidents.

Table 1 DSO's energy infrastructure parameters (state on *December* 31, 2017)

Parameter	Value
Total area	57,940 km^2
Number of end-customer	$5.5 \cdot 10^6$
Transmitted energy	45 TWh
Length of the line calculated per track with connections including:	270,189 km
–high voltage (HV)	11,143 km
–medium voltage (MV)	64,576 km
–low voltage (LV)	109,438 km
–branches	46,587 km
–lighting network	38,445 km
Power of transformers	35,714 MVA
Number of electricity substations	59,561 items
Number of HV station/*textitMV*	487 pcs.
Number of MV/LV stations	55,898 items
Number of transformers	58,611 pcs.

This paper is organized as follows: in Sect. 1 we present a short overview about geomagnetically induced currents and their source. In Sect. 2 we characterise electrical grids in the southern Poland and describe common causes of their failures. Section 3 introduces data analysed in this paper. In Sect. 4 we depict our methods and results, as well as present a discussion of our results. Section 5 contains our conclusions.

2 Characteristics of the electrical grids in the southern Poland and common causes of their failures

The considered region of Poland includes a tree-type radial network with one-sided power supply and the possibility of reserve power supply from another supply point. It is managed by the Distribution System Operator (DSO) Tauron, which uses modern technological solutions and has the potential to guarantee customers the security of supply. In carrying out its tasks, the company operates, modernises and develops its energy infrastructure. DSO has a distribution network consisting of: power lines, branches, road lighting, power stations and distribution transformers (Table 1). The size of this network is ∼25% of the electricity grids in the entire country.

3 Data

3.1 Electrical grids failures' classification

We analyze almost two years during the solar activity cycle 24. One in an early ascending phase of the cycle, near to solar minimum: 2010 and the second, during solar maximum: 2014 (the first seven months).

In 2010 DSO registered 25,616 minor failures. The breakdowns' reasons were grouped into sixteen various categories. Their relative frequency in 2010 for the considered area shows Table 2. For statistical analysis purpose we have aggregated those causes into six, more general clusters A–F.

In *January–July* 2014 DSO noticed 30,155 minor breakdowns. The electrical grid failures' (EGF) causes were grouped into twenty nine categories. Their relative frequency in 2014 displays Table 3. For analysis purpose we have aggregated these causes into the same general clusters (A–F) as in Table 2. Some details about the failures' causes can be found in [26].

Table 2 Electrical grids disruptions' causes in southern Poland distribution network in 2010

No.	Specified reasons disruptions' causes in 2010	Cluster	Description of the cluster	Number of failures	% of failures
1	trees + plants	A	meteorological effects	1205	4.7
2	ice + rime + snow + frost			853	3.3
3	wind			134	0.5
4	atmospheric discharges			1461	5.7
			Total A	3653	14.26
5	planned breaks	B	operational shutdowns	3742	14.6
6	trial quick			4125	16.1
7	quick changeover			1977	7.7
8	repair > 3 min.			464	1.8
9	damage by the recipient on the MV			7	0.0
10	damage by an adjacent oper.			769	3.0
11	switch > 3 min.			5530	21.6
			Total B	16,614	64.86
12	digging	C	vandalism	620	2.4
13	animals			204	0.8
			Total C	824	3.22
14	aging, factory defects	D	aging	1917	7.5
15	power system protection automation errors	E	electronics devices	32	0.1
16	unidentified	F	unidentified	2576	10.1
			TOTAL	25,616	100.0

The categorisation present Figs. 1–2. The first three clusters (A–C) in Tables 2–3 can be treated as objective causes. In turn, three other groups (D–F) can be associated to space weather effects. It gives 4625 failures in 2010 and 10,656 in the first seven months of 2014, which might have a geomagnetic/solar origin, and only these failures are considered in the further analysis. All of them have been verified using meteorological data from IMGW-PIB. One can easily see that in *January–July* 2014, around the solar maximum, there are 2.3 times more breakdowns in electrical grids, which can be caused by the solar factors, than in 2010, close to the solar minimum. If data of the last five months of 2014 would be available, one can expect that the difference would be even greater. Thus, this quantitative difference can be treated as a clear sign of a dependence of failures' number from clusters D–F on the solar activity level.

3.2 Geomagnetic indexes and solar wind

We take into consideration hourly data of various parameters in 2010 and 2014. We analyze four geomagnetic indexes: *Kp*, *Dst*, *Ap* and *AE*, as well as solar wind and heliosphere properties as: strength and components of heliospheric magnetic field (HMF), solar wind: speed, temperature, density and pressure, Alfven Mach Number and electric field. Some of the studied data present Figs. 3–4.

Although the solar cycle 24 was very quiet, one can easily distinguish periods of enhanced solar and geomagnetic activity, like at the beginning of April 2010, when *Kp* index reached almost 8. During that time HMF strength increased almost three and a half times during only five hours, reaching value 18.8 nT at noon on 5th of *April*. Bz component was very changeable during this time interval, varying from −7 nT up to 11.5 nT. Solar wind speed grew almost twice up to 814 km/s in early afternoon on 5th of *April*. Even more pronounced effect was visible in solar wind temperature which increased from less than 200,000 K up to more than 1,000,000 K during few hours. Solar wind density grew three
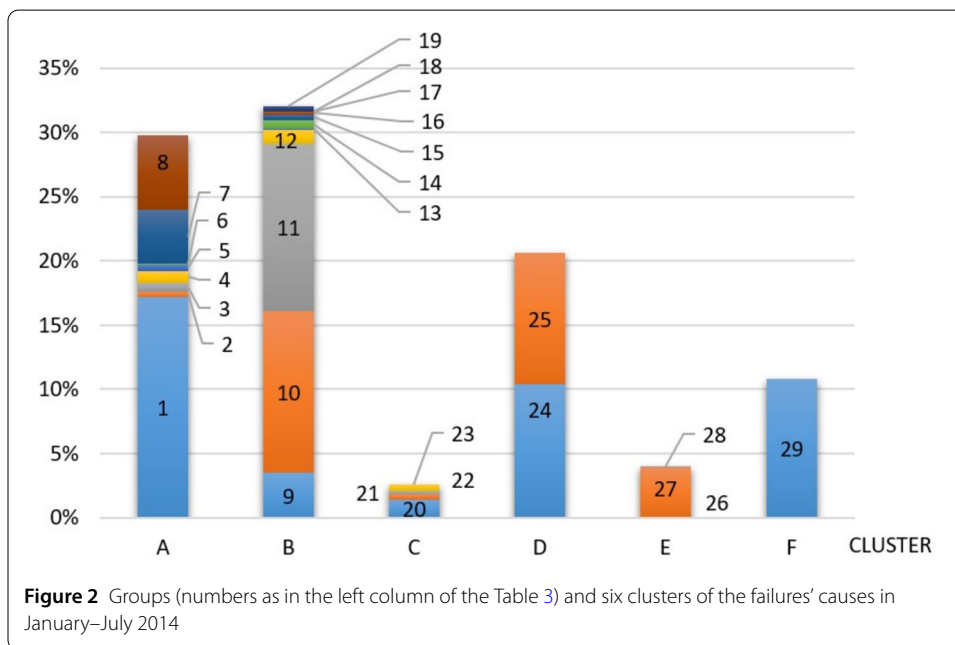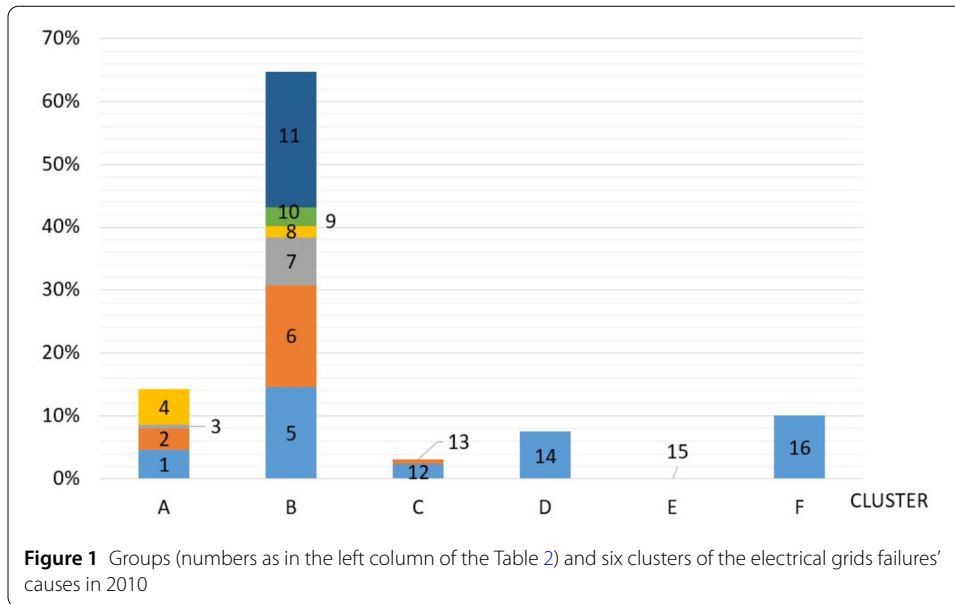
Table 3 Electrical grids disruptions' causes in southern Poland distribution network in *January–July* 2014

No.	Specified reasons disruptions' causes in 2014	Cluster	Description of the cluster	Number of failures	% of failures
1	storm	A	meteorological effects	5195	17.2
2	ice + snow + rime			124	0.4
3	rime			197	0.7
4	rime + tree + branch			271	0.9
5	snow			154	0.5
6	snow + tree + branch			30	0.1
7	wind			1272	4.2
8	wind + tree + branch			1761	5.8
			Total A	9004	29.8
9	protection devices	B	operational shutdowns	1065	3.5
10	switching			3800	12.6
11	planned breaks			3924	13.0
12	another operator			337	1.1
13	works of own brigades			38	0.1
14	open object			193	0.6
15	closed object			160	0.5
16	at the recipient			69	0.2
17	in order to save people			1	0.0
18	switching activities			6	0.0
19	assembly defects			110	0.4
			Total B	9703	32.0
20	charges, theft, disassembly	C	vandalism	410	1.4
21	cutting down trees/other parties			132	0.4
22	fire			105	0.3
23	digging			145	0.5
			Total C	792	2.6
24	aging	D	aging	3135	10.4
25	local impairment of insulation			3074	10.2
			Total D	6209	20.6
26	fuse	E	electronics devices	1	0.0
27	power system protection automation and telemechanics			1178	3.9
28	secondary circuits and power			2	0.0
			Total E	1181	3.91
29	unidentified	F	unidentified	3266	10.8
			TOTAL	30,155	100.0

times up to 12 n/cc at noon on 5th of *April*. Exactly at the same time electric field dropped to −8.6 mV/m and was very variable during this period. Moreover, on 3rd of *April* at 10:33 UT the Halo CME occurred with preceding solar flare having the onset at 9:04 UT. CME apparent speed was 668 km/s and space speed 939 km/s. All of the above mentioned effects had their reflections in the geomagnetic indexes alterations. *Ap* index increased from around 15 nT up to almost 180 nT in the morning of 5th of *April*. At the same time *AE* index exceeded 1400 nT. One day later, in the early afternoon of 6th of *April Dst* index dropped around four times to −81 nT. This type of events are the subject of our statistical. We pay attention to the events of geomagnetic storms starting from moderate ones ($Kp \geq 5$). In 2010 there were observed 11 days with maximal *Kp* index value not less than five and 7 days in *January–July* 2014 (in the whole 2014: 12 days).
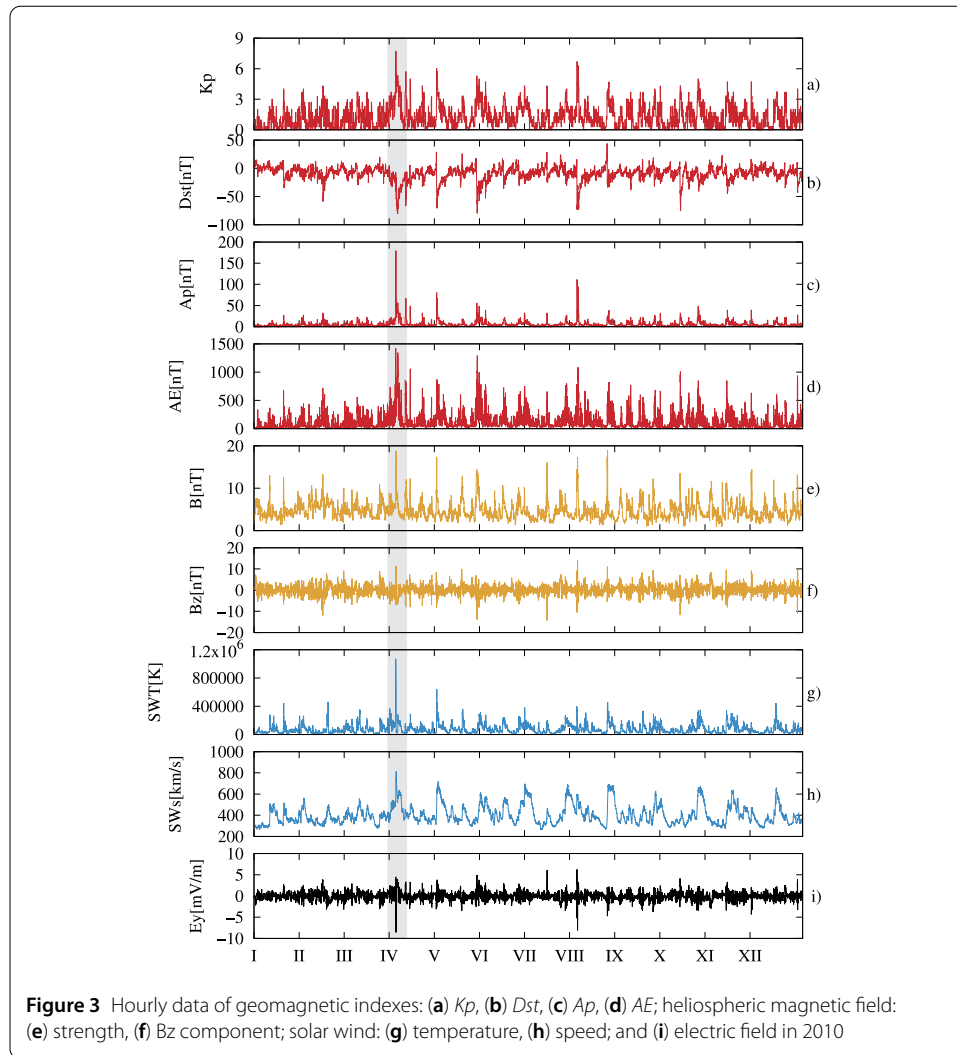
3.3 Coronal mass ejections

We analyze properties of all coronal mass ejections gathered in CME Catalog—CDAW Data Center (cdaw.gsfc.nasa.gov), recognized by hand since 1996 using LASCO instru-

Figure 1 Groups (numbers as in the left column of the Table 2) and six clusters of the electrical grids failures' causes in 2010

Figure 2 Groups (numbers as in the left column of the Table 3) and six clusters of the failures' causes in January–July 2014

ment (the Large Angle and Spectrometric Coronagraph) on board of SOHO mission (the Solar and Heliospheric Observatory). LASCO functions with three telescopes: C1, C2, and C3. Nevertheless, C1 was put out of action in June 1998. Hence, only C2 and C3 data are used for uniformity [27].

CMEs are extraordinarily widespread eruptions of plasma and magnetic field from solar corona, often succeeding solar flares, sometimes connected to solar energetic particles (SEP, e.g. [28, 29]). During 2010 there are published 1119 CMEs and in the whole year 2014: 2599. From those comprehensive lists we distinguish the so called Halo CME, i.e. coronal mass ejecta with an apparent width equal 360 deg. This type of CMEs are only ~3% of the whole population of CMEs and are an energetic population. It is worth mentioning

Figure 3 Hourly data of geomagnetic indexes: (**a**) *Kp*, (**b**) *Dst*, (**c**) *Ap*, (**d**) *AE*; heliospheric magnetic field: (**e**) strength, (**f**) Bz component; solar wind: (**g**) temperature, (**h**) speed; and (**i**) electric field in 2010
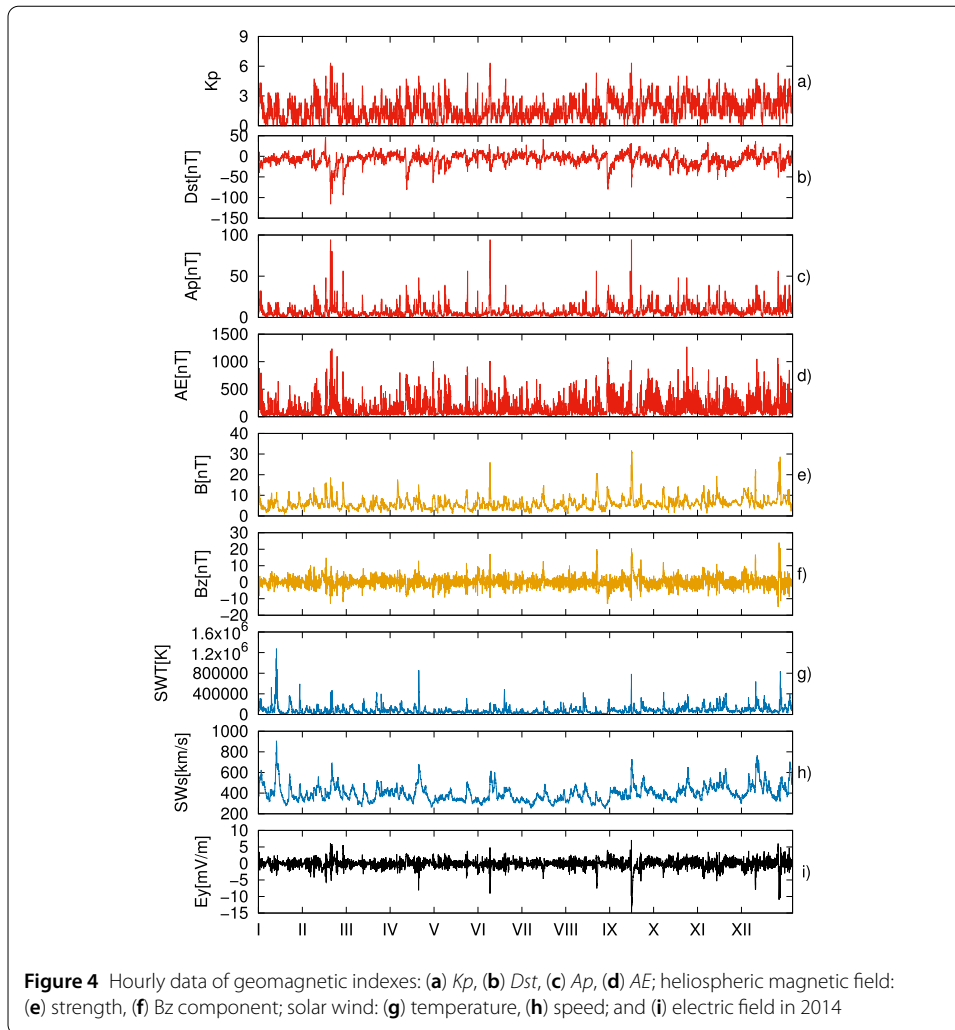
that Halo CMEs are most of the coronal mass ejections that yield huge SEP events and major geomagnetic storms [30]. In 2010 there were noticed 11 Halo CMEs (0.98% from the whole list of CMEs) and in the whole year 2014: 69 (2.65%). From these subsets we have chosen the fastest Halo CMEs, with an apparent speed or a space speed greater than 750 km/s. In our computations we consider 6 days with the fastest Halo CME in 2010 and 30 days in *January–July* 2014. Hence, during the first seven months of 2014, which was a time interval around solar maximum, there were five times more of fast Halo CME occurrence than in the whole 2010, i.e. close to the solar minimum epoch. It is worth underlying that this proportion is consistent with a difference described in the Sect. 4.1 visible in the number of electrical grids failures (EGFs) which can have solar/geomagnetic origin.

3.4 Sudden storm commencements

Sudden commencement is an abrupt and sharp growth in the northern magnetic component for particular observatory. Typically, sudden commencement occurs as a precursor of geomagnetic storm [31]. We take into consideration list of sudden storms commencement (SSC) from Ebre Observatory (http://www.obsebre.es/ca). We analyze events of 20

Figure 4 Hourly data of geomagnetic indexes: (**a**) *Kp*, (**b**) *Dst*, (**c**) *Ap*, (**d**) *AE*; heliospheric magnetic field: (**e**) strength, (**f**) Bz component; solar wind: (**g**) temperature, (**h**) speed; and (**i**) electric field in 2014

sudden storm commencements: 6 in 2010 and 14 in the first seven months of 2014, where during the whole 2014 there were 23 SSC. The contributing observatories are: Alibag and Hyderabad in India, Honolulu and San Juan in USA, Kanoya in Japan and Mbour in Senegal. Once again, the difference between the number of SSC during the first seven months of 2014 and in the whole 2010 is obvious, being 2.3 greater around solar maximum epoch, with a clear consistency with the difference pronounced in the Sect. 4.1, in the EGFs' number.

4 Methods, results and discussion

4.1 Superposed epoch analysis

Superposed epoch analysis is a method reviling relationships between the analyzed time series [32]. This tool was formerly used to investigate complex magnetospheric disturbances and peculiarities. [33], examining the correlation of the geomagnetic storm phase with a temporal variation of plasma, found at geosynchronous orbit, showed that the one of the key factors for the plasma sheet density is solar cycle. [34] studied magnetic storms' features in the relation of time of occurrence, as well as their strength. [35] analyzed (as a function of local and epoch time) the temporal evolution of geosynchronous plasma

parameters. [24] investigated dynamics of large-scale solar wind streams (corotating interaction regions, interplanetary coronal mass ejections and interplanetary shocks).

In order of performing Superposed epoch analysis, among the data of geomagnetic indexes, sudden storm commencements, as well as the fast Halo CMEs occurrence, we define the so called zero days as a key time. Next, we compose Cartesian product $(\mathbb{G}, \mathbb{F})$ of two sets of considered data series: $\mathbb{G}$ = {geomagnetic index $Kp \geq 5$; sudden storm commencements; fast Halo CMEs' occurrence} combined with $\mathbb{F}$ = {number of electrical grids failures (EGFs) caused by the aging of electrical grids elements; number of EGFs having unidentified reasons; number of EGFs caused by the electronic devices breakdowns} a matrix $\mathbb{M}$ of $m \times (a + b + 1)$ dimension. As m we define the total number of zero days connected to a particular element of the set $\mathbb{G}$, a is a number of days before the zero-day and b is a number of days after the zero-day. Elements of the matrix $\mathbb{M}$ ($\mathbb{M}_{i,j}$, where $i = 1, \ldots, m; j = 1, \ldots, a + b + 1$) are numbers of the EGFs of particular type from the set $\mathbb{F}$. Next we perform superposition of epochs (for each *j*) synchronizing all zero days: $\sum_{i=1}^{m} \frac{\mathbb{M}_{i,j} - \mathbb{M}_{i(\text{avarage})}}{\mathbb{M}_{i(\text{avarage})}}$. Samples of our results show Fig. 5.

Figures 5(a), (b), (f) present that the day after the fast Halo CME occurrence the superposed number of electrical grids failures caused by the electronic devices breakdowns, as well as having unidentified reasons increased around two and a half times from the average. Figures 5(c), (d) display that the day after and on the zero-day of *Kp* maximal value just exceeded 5 the superposed number of EGFs caused by the aging of electrical grids elements increased from 1.5 in 2010 up to 2.5 in *January–July* 2014. Figure 5(e) shows that in 2010 at the day of sudden storm commencement the superposed number of EGFs having unidentified reasons increased around twice from the average.
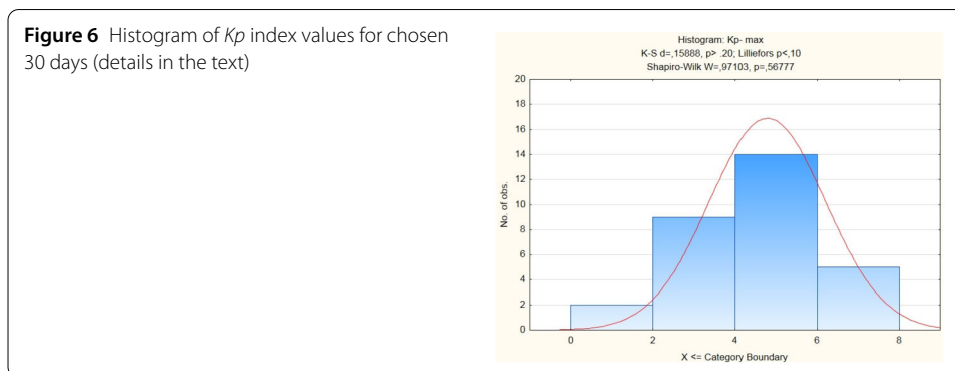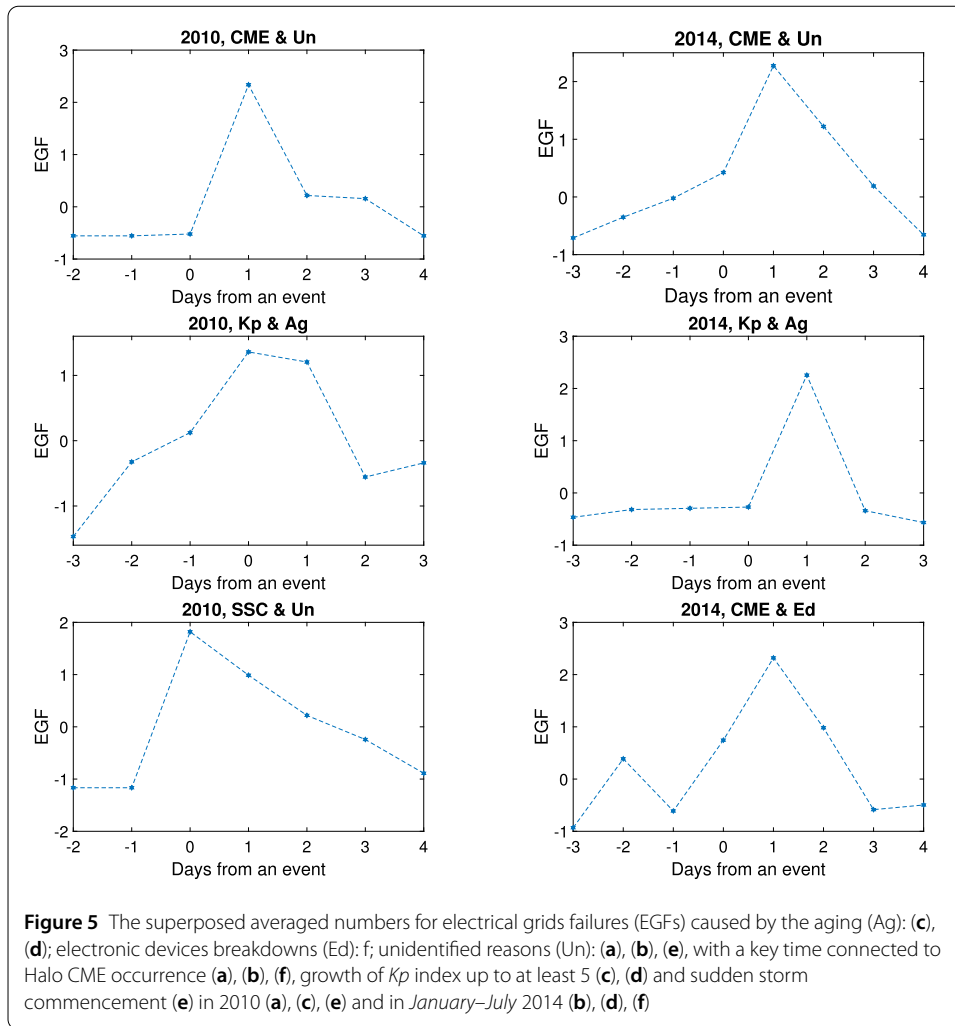
4.2 Descriptive statistics

To strengthen our results presented in Sect. 4.1 we use various statistical quantitative tools to verify a relationship between growth of *Kp* index value and failures of electrical grids' elements caused by the aging, electronic devices breakdowns or having an unidentified reasons.

We consider 3-hours data of *Kp* index from Potsdam (GFZ German Research Centre for Geosciences) for studied time intervals. To gain a daily resolution of *Kp* index data we take into account a maximal value during each considered day. Since the geomagnetic storms start from *Kp* = 5, we choose for further analysis only those days, and, based on the results presented in Sect. 4.1, the day after. Thus, we deal with $n_0 = 30$ days, for joined time intervals, 2010 and *January–July* 2014.

We apply nonparametric tests, as χ^2 test, Kolmogorov–Smirnov test (for big statistical samples) and Shapiro–Wilk W test (for small statistical samples) to prove a normality of data distribution, which is a common condition for basic statistical analysis [36]. Figure 6 presents the distribution of selected *Kp* index values having the normal form. Throughout Shapiro–Wilk test, here, $W = 0.97103$ and $p = 0.57 > \alpha = 0.05$, we confirm hypothesis H_0 that values of *Kp* index for considered 30 days has the normal distribution (Fig. 7).

Neither the data of failures caused by the electrical grids elements' aging, nor having the unidentified reasons have normal distributions. This fact confirms Shapiro–Wilk test ($\alpha = 0.05$). The values of Shapiro–Wilk test are given as $W = 0.6269$ with $p = 0.00000 < 0.05$ and $W = 0.4874$ with $p = 0.00000 < 0.05$, for failures linked to the aging and having

Figure 5 The superposed averaged numbers for electrical grids failures (EGFs) caused by the aging (Ag): (**c**), (**d**); electronic devices breakdowns (Ed): f; unidentified reasons (Un): (**a**), (**b**), (**e**), with a key time connected to Halo CME occurrence (**a**), (**b**), (**f**), growth of *Kp* index up to at least 5 (**c**), (**d**) and sudden storm commencement (**e**) in 2010 (**a**), (**c**), (**e**) and in *January–July* 2014 (**b**), (**d**), (**f**)

Figure 6 Histogram of *Kp* index values for chosen 30 days (details in the text)

the unidentified causes, respectively. It establishes that a null hypothesis on normal distribution for breakdowns connected with the aging and having the unidentified reasons has to be rejected (Fig. 8–9).

Results of the next statistical test for simplicity sake we present only for *Kp* index connections and electrical grids failures caused by the aging of the elements. Here, we consider only days with maximal *Kp* index values equal at least five and the number of electrical

Figure 7 Normal probability plot of selected *Kp* index values
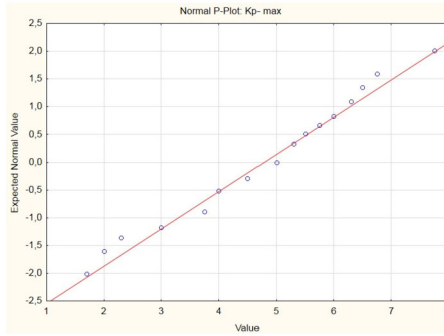
Figure 8 Histogram of the electrical grids' breakdowns number caused by the aging for chosen 30 days
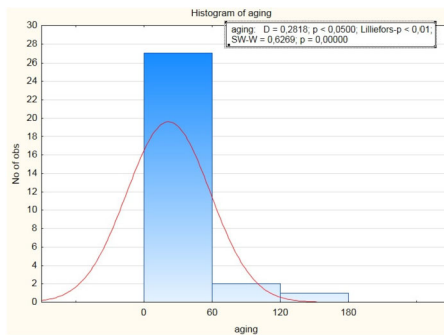
Figure 9 Histogram of the electrical grids' breakdowns number having the unidentified reasons for chosen 30 days
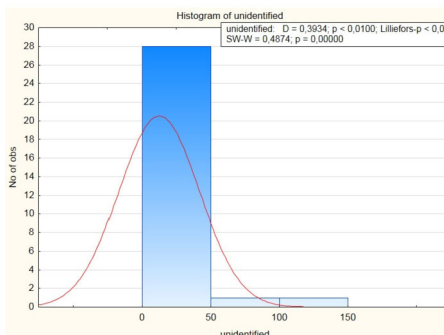
grids failures caused by the aging on the day after that. We aggregate data for $5 \leq Kp < 8$ into two groups: X, with $5 \leq Kp < 6$ and Y, with Kp index values ≥ 6. By Shapiro–Wilk test we check the normality of the distribution for both groups, we obtain the following values ($\alpha = 0.05$): $W_X = 0.6464$ with $p = 0.0001 < 0.05$ and $W_Y = 0.8812$ with $p = 0.2744 > 0.05$, for X and Y groups, respectively. We draw a conclusion that assumption on normal distribution is fulfilled only for Y group. Next, by Wilcoxon Matched Pairs Test [36] we compare the number of electrical grids failures caused by the aging in both groups, X and Y. Generally, in the Wilcoxon test H_0 hypothesis is formulated in the following way: $F_X = F_Y$, where F_X and F_Y means cumulative distribution function of group X and Y, respectively, i.e., there is no significant difference in variables' distributions of two groups X and Y, whereas H_1: $F_X \neq F_Y$.

Principally, from t-Student distribution table we find a critical value $T_{\alpha,n}$ for a given level of significance α and for n degrees of freedom (n is the number of these cases which are

Figure 10 Wilcoxon Matched Pairs Test results for *X* (failures linked to the days with $5 \leq Kp < 6$) and *Y* (with *Kp* index values ≥ 6) groups, where *Z* means the statistic value of the Wilcoxon test when $n > 25$

really calculated). The critical set for this test is $[0, T_{\alpha,n}]$. If $T > T_{\alpha,n}$ we have no bases to reject hypothesis H_0.

Our computations show that with $p = 0.0464$ the statistic value equals $T = 1$, whilst $T_{\alpha=0.05,n=6} = 2.447$ hence, we reject H_0 and put H_1, which means that variables' distributions in groups *X* and *Y* differ significantly (Fig. 10). It means that the higher value the Kp index was, the greater the number of electrical grids' failures of the aging type was recorded.

4.3 Discussion

Solar cycle 24 belongs to the less active, comparable with cycles from the beginning of the twenty century. During this cycle not many spectacular storms occurred, and non of them could be compared to, for instance, Halloween Storm.

For studied time intervals we have distinguished eighteen days with maximum value of *Kp* index not less than five. Based on the LASCO CME catalogue we have considered thirty six Halo CMEs with an apparent speed or a space speed greater than 750 km/s. Using list of sudden storm commencements we took into account twenty events. Figure 5 shows that the growth in the superposed averaged number of electrical grids breakdowns appears around one day after the fast Halo CME occurrence. Moreover, the fast increase in the superposed averaged number of failures occurs on the day of SSC, as well as around zero-day or the day after when the Kp index value was greater or equal 5. The increase of the superposed EGFs number varies from 1.5 up to 2.5. Those results are strengthened by the statistical hypotheses tests (Fig. 10).

Hence, the electrical grids in southern Poland were influenced by GIC, which were generated by the powerful phenomena having solar origin and caused structural changes in the inner heliosphere, and consequently, in the geosphere.

5 Conclusions

1. Comparing the total number of electrical grids failures near the solar minimum (2010) and around the solar maximum (*January–July* 2014) the quantity of failures is twice greater during the first seven months of 2014 than in 2010. It can be treated as an indicator of solar cycle phase dependence.

2. The increase in the superposed averaged number of electrical grids failures appears around one day after the fast Halo CME occurrence.

3. The rapid growth in the superposed averaged number of electrical grids failures occurs on the day of SSC, as well as around zero-day or the day after when the geomagnetic *Kp* index was greater or equal 5.

4. Presented results confirm that influential phenomena having solar origin, affected in 2010 and *January–July* 2014 the efficiency of the electrical grids in southern Poland.

Abbreviations
CME, Coronal Mass Ejection; DSO, Distribution System Operator; EGF, Electrical Grid Failures; GIC, Geomagnetically Induced Currents; HMF, Heliospheric Magnetic Field; HF, High Frequency; HV, High Voltage; IMGW-PIB, The Institute Of Meteorology And Water Management-National Research Institute; LASCO, The Large Angle And Spectrometric Coronagraph; LV, Low Voltage; MV, Medium Voltage; SA, Solar Activity; SEP, Solar Energetic Particles; SF, Solar Flare; SSC, Sudden Storms Commencement.

Availability of data and materials
Heliospheric and geomagnetic parameters are publicly available at: http://www.gfz-potsdam.de, http://omniweb.gsfc.nasa.gov, http://cdaw.gsfc.nasa.gov and http://www.obsebre.es.

Competing interests
The authors declare that they have no competing interests.

Authors' contributions
AG planned the scientific content, done analysis performed in the Sect. 4.1, prepared and described most of the data for Sects. 3.2–3.4, the discussion of the results presented in the article. RM coauthor of the introduction and Figs. 3–4. SM collected data of electrical grids failures. AS done analysis performed in the Sect. 4.2. MS author of the Sect. 2 and Sect. 3.1, collected data of electrical grids failures. AW coauthor of the introduction and Figs. 3–4. SZ collected data of Kp index from GZF-Potsdam. All authors read and approved the final manuscript.

Author details
[1]Institute of Mathematics and Physics, Siedlce University, Siedlce, Poland. [2]Department of Electrical and Power Engineering, AGH University of Science and Technology, Krakow, Poland. [3]Institute of Computer Sciences, Siedlce University, Siedlce, Poland. [4]Institute of Social Science and Security, Siedlce University, Siedlce, Poland.

Publisher's Note
Springer Nature remains neutral with regard to jurisdictional claims in published maps and institutional affiliations.

References
1. Hathaway DH. The solar cycle. Living Rev Sol Phys. 2015;12(4). https://doi.org/10.1007/lrsp-2015-4.
2. Parker EN. Dynamics of the interplanetary gas and magnetic fields. Astrophys J. 1958;128(1):664. https://doi.org/10.1086/146579.
3. Eastwood J-P, Biffis E, Hapgood MA, Green L, Bisi MM, Bentley RD, Wicks R, McKinnell LA, Gibbs M, Burnett C. The economic impact of space weather: where do we stand?. Risk Anal. 2017;37(2). https://doi.org/10.1111/risa.12765.
4. Marusek JA. Solar storm threat analysis, http://www.breadandbutterscience.com/SSTA.pdf. 2007.
5. Balogh A, Hudson HS, Petrovay K, von Steiger R. Introduction to the solar activity cycle: overview of causes and consequences. In: Balogh A, Hudson H, Petrovay K, von Steiger R, editors. Space sciences series of ISSI. New York: Springer; 2014. p. 1–15.
6. Gonzalez WD, Tsurutani BT. Criteria of interplanetary parameters causing intense magnetic storms (Dst of less than −100 nT). Planet Space Sci. 1987;35:1101–9. https://doi.org/10.1016/0032-0633(87)90015-8.
7. Cannon PS. Extreme space weather. A report published by the UK Royal Academy of Engineering. Space Weather. 2013;11(4):138–9. https://doi.org/10.1002/swe.20032.
8. Viljanen A, Pirjola R. Geomagnetically induced currents in the Finnish high-voltage power system. Surv Geophys. 1994;15(4):383–408. https://doi.org/10.1051/swsc/2014006.
9. Pirjola R. Geomagnetically induced currents during magnetic storms. IEEE Trans Plasma Sci. 2000;28(6):1867–73. https://doi.org/10.1109/27.902215.
10. Choi HS, Lee J, Cho KS, Kwak YS, Cho IH, Park YD, Kim YH, Baker DN, Reeves GD, Lee DK. Analysis of GEO spacecraft anomalies: space weather relationships. Space Weather. 2011;9(6):S06001. https://doi.org/10.1029/2010SW000597.
11. Dyer CS, Lei F, Clucas SN, Smart DF, Shea MA. Solar particle enhancements of single-event effect rates at aircraft altitudes. IEEE Trans Nucl Sci. 2003;50(6):2038–45. https://doi.org/10.1109/TNS.2003.821375.
12. Wik M. The sun, space weather and effects. Phd Thesis. 2008.
13. Campbell WH. An interpretation of induced electric currents in long pipelines caused by natural geomagnetic sources of the upper atmosphere. Surv Geophys. 1986;8(3):239–59. https://doi.org/10.1007/BF01904061.
14. Pulkkinen A, Viljanen A, Pajunpaa K, Pirjola R. Recordings and occurrence of geomagnetically induced currents in the Finnish natural gas pipeline network. J Appl Geophys. 2001;48(4):219–31. https://doi.org/10.1016/S0926-9851(01)00108-2.
15. Gaunt CT, Coetzee G. Transformer failures in regions incorrectly considered to have low GIC-risk. In: 2007 IEEE Lausanne power tech. 2007. p. 807–12.

16. Gaunt CT. Reducing uncertainty—responses for electricity utilities to severe solar storms. J Space Weather Space Clim. 2014;4:7. https://doi.org/10.1051/swsc/2013058.

17. Bolduc L. GIC observations and studies in the Hydro-Quebec power system. J Atmos Sol-Terr Phys. 2002;64(16):1793–802. https://doi.org/10.1016/S1364-6826(02)00128-1.

18. Baker DN, Balstad R, Bodeau JM, Cameron E, Fennell JF, Fisher GM, Forbes KF, Kintner PL, Leffler LG, Lewis WS, Reagan JB, Small AA III, Stansell TA, Strachan L Jr., Graham SJ, Fisher TM, Swisher V, Gruber CA. Severe space weather events–understanding societal and economic impacts: a workshop report. In: Committee on the societal and economic impacts of severe space weather events: a workshop. Washington: Space Studies Board, National Research Council; 2008. p. 29–49.

19. Thorberg R. Risk analysis of geomagnetically induced currents in power systems. Report Lund University. 2012.

20. Pulkkinen A, Lindahl S, Viljanen A, Pirjola R. Geomagnetic storm of 29–31 October 2003: geomagnetically induced currents and their relation to problems in the Swedish high-voltage power transmission system. Space Weather. 2005;3(8). https://doi.org/10.1029/2004SW000123.

21. Colak T, Qahwaji R. Automated prediction of solar flares using neural networks and sunspots associations. In: Saad A, Dahal K, Sarfraz M, Roy R, editors. Soft computing in industrial applications. Advances in soft computing, vol. 39. Berlin: Springer; 2007. p. 316–24.

22. Reikard G. Forecasting space weather: can new econometric methods improve accuracy? Adv Space Res. 2011;47(12):2073–80. https://doi.org/10.1016/j.asr.2011.03.037.

23. Caswell JM. A nonlinear autoregressive approach to statistical prediction of disturbance storm time geomagnetic fluctuations using solar data. J Signal Inf Process. 2014;5:42–53. https://doi.org/10.4236/jsip.2014.52007.

24. Yermolaev YI, Lodkina IG, Nikolaeva NS, Yermolaev MY. Dynamics of large-scale solar wind streams obtained by the double superposed epoch analysis. J Geophys Res Space Phys. 2015;120(9):7094–106. https://doi.org/10.1002/2015JA021274.

25. Camporeale E, Wing S, Johnson J. Machine learning techniques for space weather. Amsterdam: Elsevier; 2018.

26. Moskwa S, Koziel S, Siluszyk M, Galias Z. Zastosowanie modelu pogodowego w optymalizacji lokalizacji punktow rozciec w sieciach dystrybucyjnych. Przeglad Elektrotechniczny. 2019;95(2):117–22. https://doi.org/10.1109/TNS.2003.821375.

27. Yashiro S, Gopalswamy N, Michalek G, Cyr OCS, Plunkett SP, Rich NB, Howard RA. A catalog of white light coronal mass ejections observed by the SOHO spacecraft. J Geophys Res Space Phys. 2004;109. https://doi.org/10.1029/2003JA010282.

28. Kahler SW, White SM, Ling AG. Forecasting E > 50-MeV proton events with the proton prediction system (PPS). J Space Weather Space Clim. 2017;7. https://doi.org/10.1051/swsc/2017025.

29. Prakash O, Feng L, Michalek G, Gan W, Lu L, Shanmugaraju A, Umapathy S. Characteristics of events with metric-to-decahectometric type II radio bursts associated with CMEs and flares in relation to SEP events. Astrophys Space Sci. 2017;362(3). https://doi.org/10.1007/s10509-017-3034-y.

30. Gopalswamy N, Akiyama S, Yashiro S, Makela P. Coronal mass ejections from sunspot and non-sunspot regions. In: Magnetic coupling between the interior and atmosphere of the sun: proceedings of the conference "centenary commemoration of the discovery of the evershed effect". 2008. p. 289–307.

31. Curto JJ, Araki T, Alberca LF. Evolution of the concept of sudden storm commencements and their operative identification. Earth Planets Space. 2007;59(11):i–xii. https://doi.org/10.1186/BF03352059.

32. Chree C. Some phenomena of sunspots and of terrestrial magnetism at kew observatory. Philos Trans R Soc Lond Ser A. 1913;212:75–116. https://doi.org/10.1098/rsta.1913.0003.

33. Denton MH, Thomsen MF, Korth H, Lynch S, Zhang JC, Liemohn MW. Bulk plasma properties at geosynchronous orbit. J Geophys Res Space Phys. 2005;110(6). https://doi.org/10.1029/2004JA010861.

34. Liemohn MW, Zhang JC, Thomsen MF, Borovsky JE, Kozyra JU, Ilie R. Plasma properties of superstorms at geosynchronous orbit: how different are they?. Geophys Res Lett. 2008;35(6). https://doi.org/10.1029/2007GL031717.

35. Ilie R, Liemohn MW, Thomsen MF, Borovsky JE, Zhang J. Influence of epoch time selection on the results of superposed epoch analysis using ACE and MPA data. J Geophys Res Space Phys. 2008;113. https://doi.org/10.1029/2008JA013241.

36. Shao J. Mathematical statistics. New York: Springer; 2003.